Korean J. Chem. Eng., 34(8), 2301-2310 (2017)
DOI: 10.1007/s11814-017-0114-1

pISSN: 0256-1115
eISSN: 1975-7220

Anti-corrosive performance of epoxy coatings containing various nano-particles for splash zone applications

Mohammad Asif Alam*, Ubair Abdus Samad*, Rawaiz Khan, Manawwer Alam***,†, and Saeed Mohammed Al-Zahrani****

*Center of Excellence for Research in Engineering Materials (CEREM), Advanced Manufacturing Institute (AMI), King Saud University, P. O. Box 800, Riyadh-11421, Saudi Arabia
**Chemical Engineering Department, King Saud University, P. O. Box 800, Riyadh-11421, Saudi Arabia
***Research Centre-College of Science, King Saud University, P. O. Box 2455, Riyadh-11451, Saudi Arabia
(*Received 3 November 2016 • accepted 18 April 2017*)

Abstract−Various formulations of epoxy nano-composites coating were developed by incorporating the nanoparticles (NPs) of ZnO, ZrO_2, and SiO_2 (2 wt%) in commercially available epoxy resin as the matrix phase. Direct incorporation method was used for the addition of NPs in epoxy matrix. High-speed mechanical stirring and ultra-sonication were carried out to facilitate the dispersion of NPs in the presence of acetone used as a solvent. Coating of neat epoxy and NPs (ZnO, ZrO_2, SiO_2) doped coating was applied on mild steel substrate for corrosion analysis. The effect of the incorporation of various NPs on anti-corrosive properties of the epoxy/nano-composite coatings was investigated by electrochemical impedance spectroscopy technique. The experimental results showed an improvement in the anticorrosive properties for EZr coatings as compared with pristine and other nanocomposite coating samples.

Keywords: Nanoparticles, Epoxy, Nanocomposite Coating, Electrochemical Impedance Spectroscopy (EIS)

INTRODUCTION

In this advanced technological era corrosion is still considered a major problem because it is the main cause of industrial failures and loss of billions of dollars annually for preventive maintenance and restoration of metal substrates [1]. There are many processes introduced by researchers to overcome this phenomenon or to slow down the process of corrosion. Nowadays, several polymeric coatings are used to protect the substrate [2-5], but in actual practice these polymeric coatings are vulnerable to corrosive species to a certain extent [6-10], which causes loss of adhesion, ultimately leading towards the failure of barrier coating and making substrate susceptible to corrosion. With the introduction of NPs as fillers in polymeric coating system, the efficiency of polymeric coatings in terms of corrosion resistance can be increased while improvement in mechanical properties is an added advantage, which makes them materials of choice suitable for commercial applications in automotive industries, marine, construction machineries, chemical industries etc. Several studies have been conducted on these composite coatings by selecting SiO_2 [11-14], TiO_2 [15,16], Fe_2O_3 [17], ZnO [18-20], Al_2O_3 [21,22], ZrO_2 [14,23]. Reported results suggest that the addition of these NPs improves the anticorrosion properties. These NPs impart superior properties than other fillers even when added in lower concentrations [24,25]. The only difficulty linked while using these nanosized fillers is their dispersion, which plays a major role in achieving the desired properties. Since the NPs have large surface area, they exhibit strong affinity to agglomerate [26].

Fabrication of different types of coatings depending upon application, used with and without solvent, are highlighted. Using photopolymerization technique [27-29], several authors fabricated dye-sensitized solar cell with the help of cross-linkable polymeric membrane to be used in electrochromic and photo electrochromic devices possessing increased efficiency and stability. Pureun et al. [30] fabricated successfully multifunctional optical thin film stabilized by the UV photopolymerization to achieve excellent chemical and mechanical resistance. Pintossi et al. [31] developed organic-inorganic hybrid coating for flexible organic photovoltaic devices, which exhibited multifunctional properties. Masaru et al. [32] fabricated porous anodic aluminum oxide thin films to be used in UV nanoimprinting technology using electrochemical oxidation. Apart from these technologies, some other techniques for anticorrosion coatings are also reported.

Some significant research was done previously using different NPs and their treatment before adding to matrix to avoid agglomeration, which suggested that addition of NPs possesses capability to resist corrosion and NP treatment can enhance its dispersion into epoxy matrix. Rosero et al. [11] used silica NPs in sol-gel coatings for corrosion prevention and concluded that addition of silica nanoparticles enhances corrosion resistance properties. Huang et al. [12] used SiO_2 particles synthesized by sol-gel method with epoxy resin to produce epoxy nanocomposite coatings. Electrochemical studies were carried out in 5% NaCl solution, and results revealed that coatings containing NPs gave better anticorrosion properties as compared to coatings without NPs. Shi et al. [14] used nanosized TiO_2 and SiO_2 (silane treated) along with epoxy resin and suggested that addition of 1 wt% of both NPs significantly improved the corrosion resistance (EIS and salt spray); they also concluded that ad-

†To whom correspondence should be addressed.
E-mail: malamiitd@gmail.com

dition of these NPs showed improvement in hardness. Rashvand et al. [19] prepared epoxy coating containing zinc oxide; the coatings were exposed to UV, and corrosion properties of those UV exposed coatings were evaluated using EIS. They concluded that coatings with ZnO had uniform degradation, while coating without ZnO deteriorated quickly.

The percentage of NPs used in preparing these anticorrosion coatings is also an important point needing further consideration. Previously published research suggested that the presence of higher percentage of nanoparticles in matrix resin was less effective because of the NPs tendency to agglomerate [33-35]. To avoid agglomeration of nanoparticles and surface roughness it's mandatory to achieve homogeneous dispersion of NPs. For this purpose, 2 wt% of NPs was selected, as it in compliance with the literature [34,36-38].

In our previous work [39] we studied thermo-mechanical properties of epoxy coatings containing 2 wt% of various NPs, where we explained in detail the interaction of nanoparticles according to the results obtained by characterization data. However, the focus of this work was to investigate the same coating samples for anticorrosive properties in 3.5% NaCl solution in order to assess its performance for splash zones applications. The need for this study was to compare and evaluate the functionality and effectiveness of different nanoparticles in same percentage (2 wt%) in order to replace the current anticorrosive additives which have some serious health and environmental effects. Electrochemical impedance spectroscopy (EIS) was carried out for studying the corrosion properties of the coating samples over mild steel substrates. Scanning electron microscopy coupled with energy dispersive X-ray analysis (EDX) was also performed on test specimens to analyze the distribution of NPs in epoxy matrix. The effect of NPs on surface morphology and topology was determined using SEM and atomic force microscopy (AFM).

EXPERIMENTAL AND METHOD

1. Materials

Epon (1001-k-65) with EEW (epoxy equivalent weight) of 450-550 g/equivalent and 1,500-4,500 cP Brookfield viscosity at 25 °C was used as matrix resin, purchased from Hexion Chemicals (United States). Hardener (polyaminoamide adduct R-41) was purchased from Huntsman Advanced Materials. All NPs used in this study, such as ZnO, ZrO_2 and SiO_2, were of same size, 50±5 nm, obtained from Sigma Aldrich. Acetone (Merck, 99%) was used as solvent.

2. Sample Preparation

Initially, the NPs were mixed in acetone diluted epoxy matrix for better dispersion, where the ratio of epoxy to hardener was kept at 1 : 4. The mixing was accomplished using laboratory scale mechanical mixer (Dispers Master, Sheen Instruments. Ltd., UK) at 3,000 rpm for 1 h. After complete mixing, sonication was performed at 50 °C for 90 min. Hardener was added to the mixture and stirred mechanically at 600 RPM for 30 min. Finally, the solution was left for 10 minutes for stabilization. Using a bird applicator (Sheen Instruments. Ltd., UK) with gap size of 90 μm, the slurry was directly applied on steel panels. The coated panels were placed carefully on a smooth surface to get uniform film thickness in dust-free environment. Panels were left to cure for 5 days at room temperature, prior to characterization [39].

3. Characterization

FE-SEM (JEOL JSM7600F) and EDX were used to determine surface morphology of the coatings. The microscope was operated at 5 kV with a working distance of 4.5 mm. TGA was performed by a TA Instrument SDT Q-600. The instrument was calibrated according to the manufacturer's procedure, using indium as the standard reference material. The tests were at a heating rate of 10 °C/min from room temperature to 600 °C in nitrogen atmosphere (10 ml/min). AFM involved using a TriA SPM (A.P.E. Research, Basovizza 34149, Trieste, Italy). The anticorrosive performance of epoxy coating system was investigated by EIS measurements in a conventional three electrode cell with Ag/AgCl, stainless steel, and steel coated panel. The area of working electrode that was exposed to the test solution (3.5% NaCl solution) was 10 cm^2. The EIS data were collected using an Autolab Ecochemie PGSTAT 30 (potentiostate/galvanostate) and the frequency scan was carried out by applying a ±5 mV amplitude sinusoidal wave perturbation at the corrosion potential value. The frequency range was scanned from 100 kHz to 1 MHz, and the data were recorded for five impedance points per frequency.

RESULTS AND DISCUSSION

1. FE-SEM and EDX Analysis

SEM combined with EDX analyses were used to evaluate the dispersion of NPs in epoxy matrix and confirm the presence of NPs at particular scanning area. The samples were coated with thin platinum layer to avoid charging of samples. EDX mapping was implemented on the identical position to further confirm the distribution of NPs in matrix resin. Fig. 1 shows typical scanning electron microscope images of composite coatings with (A) ESi, (B) EZn, (C) EZr NPs. All the images show smooth surface of composite coatings. Particles are uniformly distributed because of silane addition in matrix, which facilitates the mixing of NPs [40]. Dispersion of NPs is not fully homogeneous and has slight formation of aggregates. This is because NPs have a higher tendency to agglomerate, which is further evident from mapping images.

To support the dispersion of NPs in matrix resin, EDX on SEM samples were applied to detect the NPs in prepared composite coatings. EDX was performed on the same position shown in Fig. 1. Fig. 2(A')-(C') shows the EDX images of nanocomposite coatings. In all the images thathet NPs are equally distributed all over the coatings, which proves particles' uniform distribution all over the coating. Due to higher tendency of NPs to agglomerate [26], slight aggregates can be witnessed in all the samples. The obtained EDX spectra and their percentages are shown in Fig. 3 and Table 1, which also confirms the approximate 2 wt% addition of NPs in epoxy matrix resin.

2. Thermogravimetric Analysis

Fig. 4 shows TGA thermograms for the EP and nanocomposite coatings. TGA traces of the cured pristine and cured nanocomposite coatings provide information about their thermal stability and thermal degradation behavior. The results for temperature at 50% weight loss (T_{50}), initial decomposition temperature (T_i), maxi-

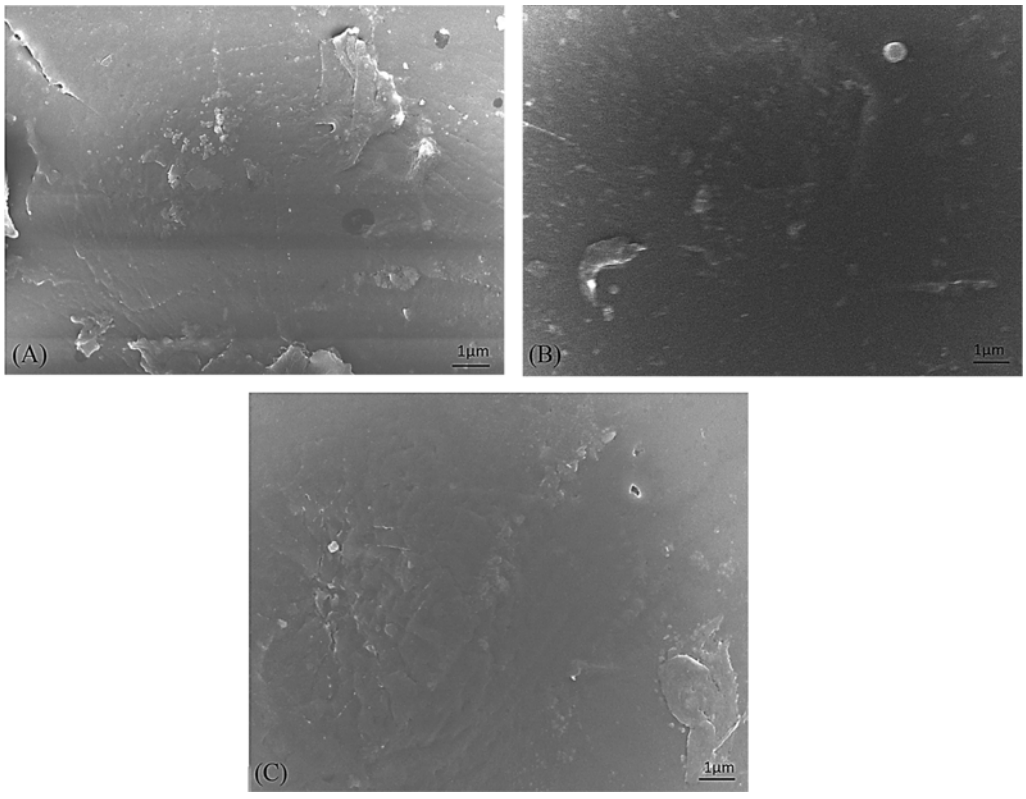

Fig. 1. Scanning Electron Microscope image of epoxy nanocomposite (A) ESi, (b) EZn, (C) EZr.

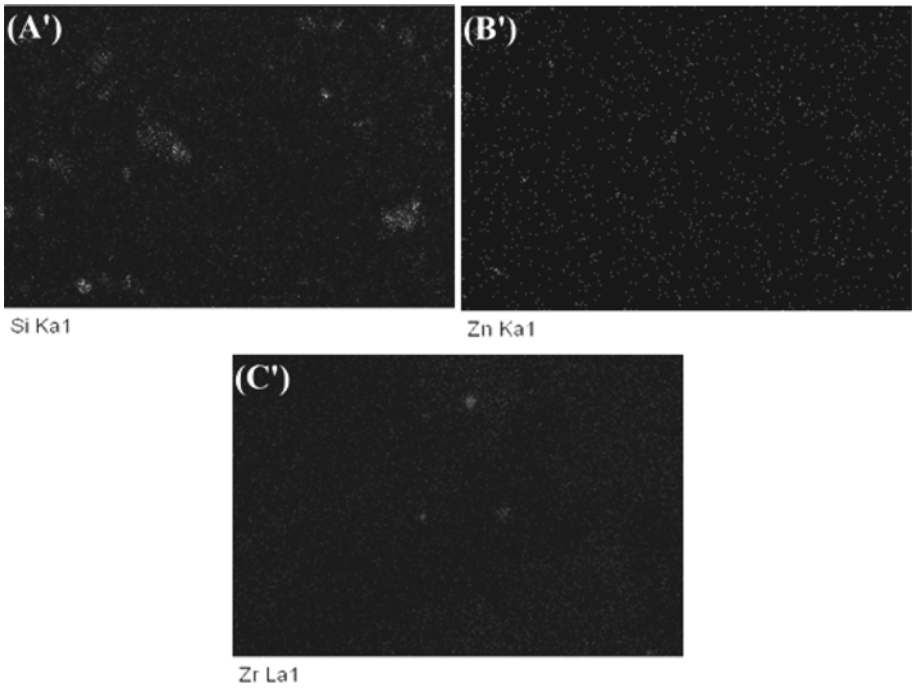

Fig. 2. Mapping images of epoxy nanocomposites (A′) ESi, (B′) EZn, (C′) EZr.

mum decomposition temperature (T_{max}) and the amount of char residual at 600 °C are summarized in Table 2 for all compositions. The higher values of T_{50} and T_{max} illustrate that ESi and EZr possess higher thermal stability as compared to EP. There are different theories regarding the effect of NPs in reinforced polymeric-inorganic nano-composites. One of these theories is the barrier model, which claims that thermal stability of such nanocomposites is improved due to the formation of strong polymeric-inorganic char [41-43].

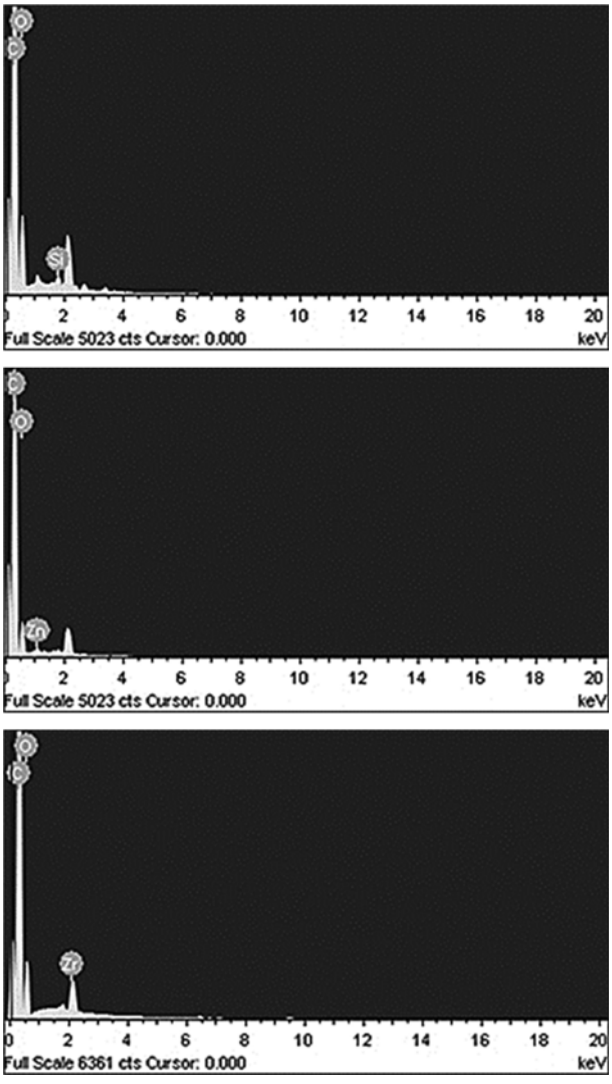

Fig. 3. EDX spectra of different NPs incorporated composite coatings.

The presence of these fillers may inhibit the molecular mobility of the polymer chains.

Moreover, the nanocomposites having higher residual char at 600 °C results in enhanced thermal stability due to the presence of NPs as in case of ESi and EZr. In ESi and EZr, the observed two-step degradation profiles suggest that the presence of SiO_2 and ZrO_2 does not lead to the changes in the degradation mechanism of the coating. However, the stability of ESi and EZr is improved due to large amount of residual char, which acts as thermal protection, resulting in higher T_{max} than the pure epoxy. However, the detailed mechanism of such a process is not well known. The improvement in thermal stability is probably due to the combined effect of a large amount of char produced along with interaction of NPs with the polymer matrix. The presence of ZnO NPs in nanocomposite may facilitate thermal degradation of epoxy resin by serving as a catalyst. The decrease in thermal degradation temperature in presence of ZnO NPs agrees with the literature, which showed a decreased thermal degradation temperature for rigid and flexible series of polyimide/ZnO hybrid coatings [44]. The same patterns of TG curves of ESi and EZr confirm that there is no change in degradation mechanism.

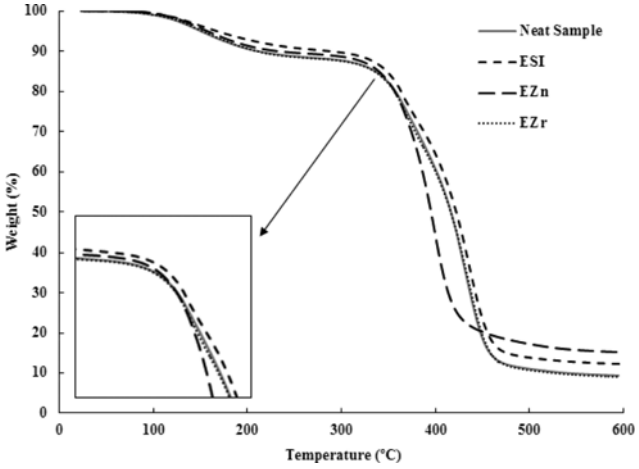

Fig. 4. TGA curves for pristine and modified epoxy coating.

Table 2. TGA results for pure and nanocomposite epoxy coatings

Coating sample	T_i (°C)	T_{50} (°C)	T_{max} (°C)	Res. char at 600 °C (wt%)
EP	364.4	416.3	431.2	9.00
EZr	364.7	419.3	435.4	10.99
EZn	364.7	394.9	398.0	9.17
ESi	359.4	421.7	436.0	12.25

3. Electrochemical Impedance Spectroscopy Analysis

To evaluate the impact of these NPs (SiO_2, ZnO, ZrO_2) on anti-

Table 1. Obtained constituents and percentages of elements after EDX analysis

Elements	ESi		EZn		EZr	
	Weight %	Atomic %	Weight %	Atomic %	Weight %	Atomic %
C	85.58	89.42	86.16	90.27	83.61	89.24
O	12.24	9.60	11.90	9.36	12.80	10.26
Si	2.18	0.98	-	-	-	-
Zn	-	-	1.94	0.37	-	-
Zr	-	-			3.58	0.50
Total	100		100		100	

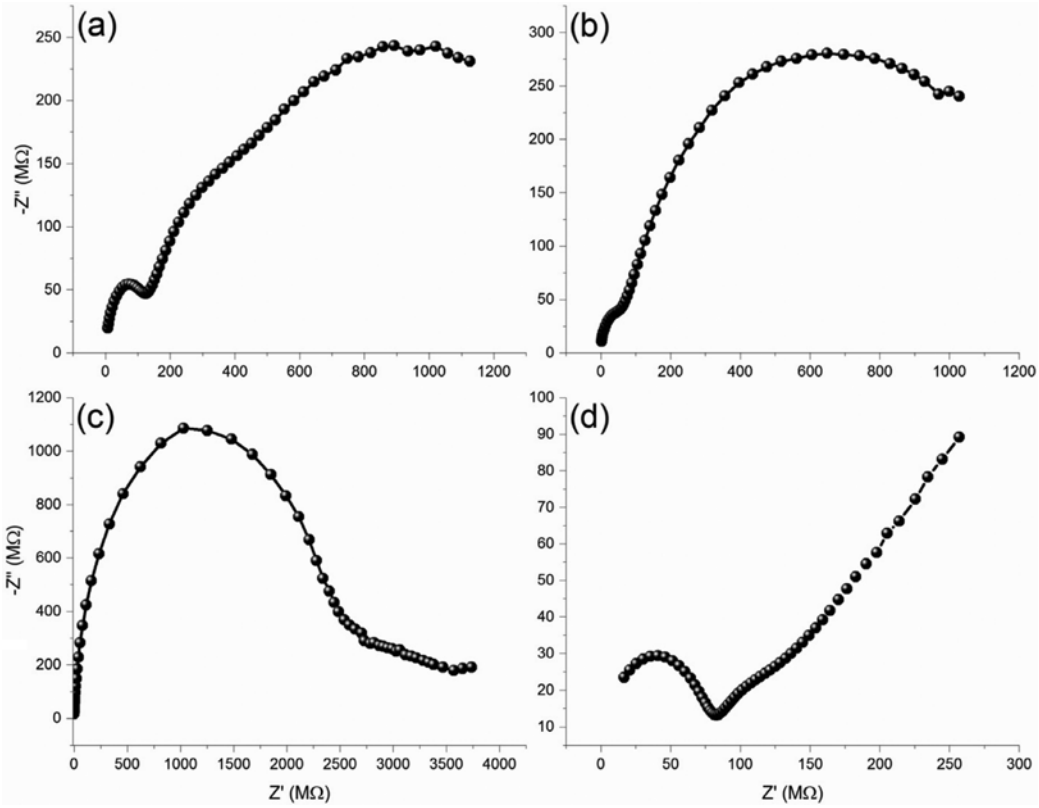

Fig. 5. Nyquist spectrum obtained after 1 h exposure in 3.5% NaCl solution (a) EP, (b) ESi, (c) EZn, (d) EZr.

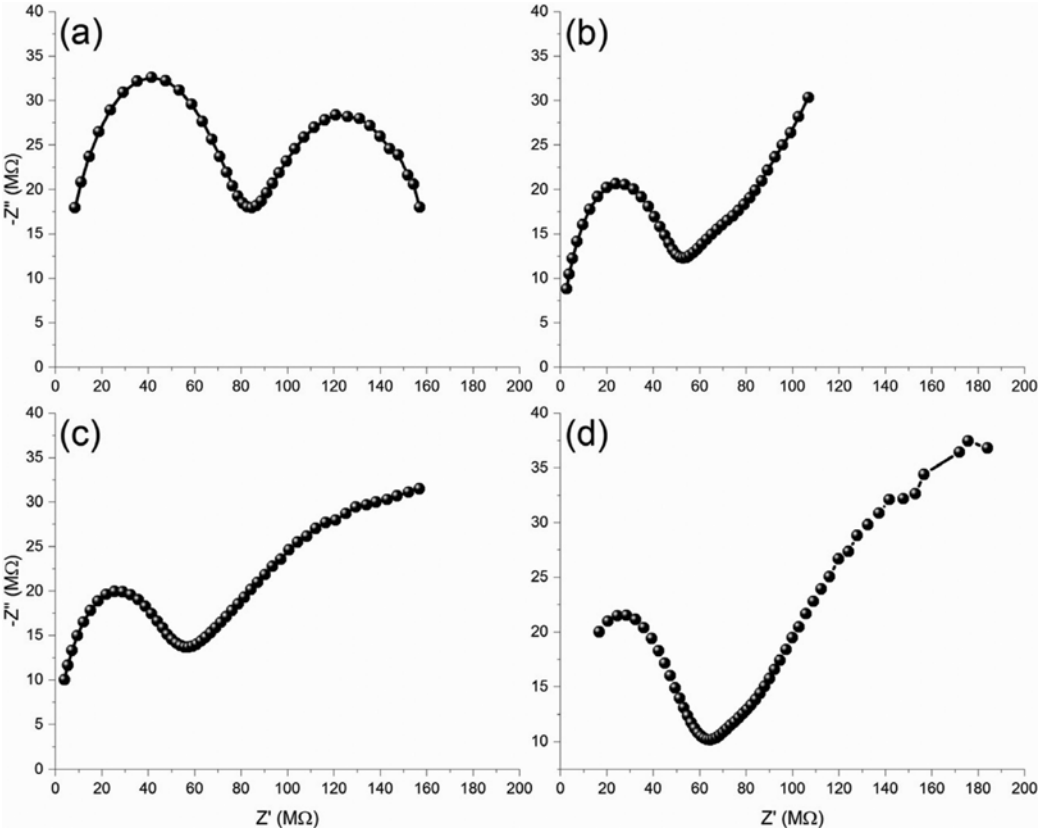

Fig. 6. Nyquist spectrum obtained after 5 day's exposure in 3.5% NaCl solution (a) EP, (b) ESi, (c) EZn, (d) EZr.

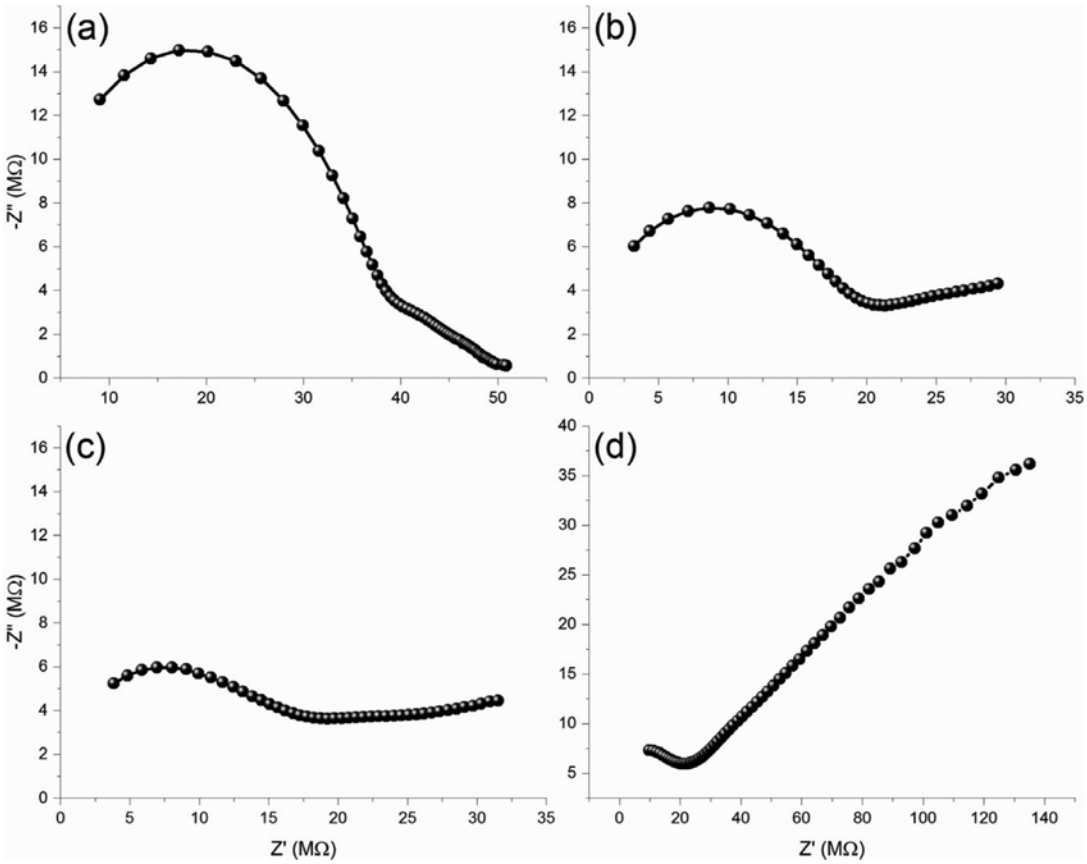

Fig. 7. Nyquist spectrum obtained after 25 days exposure in 3.5% NaCl solution (a) EP, (b) ESi, (c) EZn, (d) EZr.

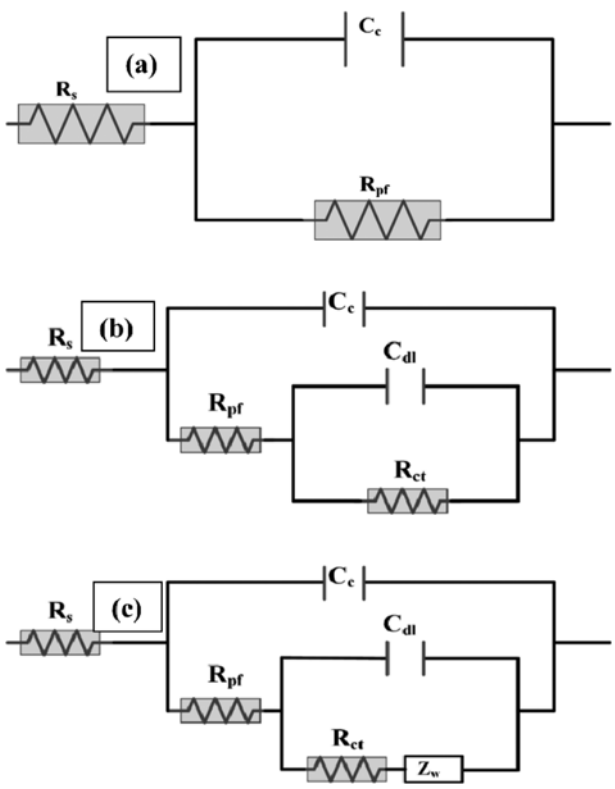

Fig. 8. Equivalent circuit used to fit Nyquist plot.

corrosion performance coatings on coated steel panels, EIS was carried out at different intervals (1, 5 and 25 days) after exposure to 3.5% NaCl solution. Fig. 5 depicts typical Nyquist plots obtained for (a) EP, (b) ESi, (c) EZn, and (d) EZr after one day of exposure to 3.5% NaCl solution. Comparable EIS experimentation was also done for the coatings in the sodium chloride solutions after 5 and 25 days of exposure, and the plots are shown in Fig. 6 and Fig. 7, respectively. To analyze the obtained Nyquist plots, various equivalent circuit models shown in Fig. 8 were used to fit the experimental data. The Nyquist plot was used to analyze the initiation of corrosion, penetration of water into coating/metal interface and formation of the corrosion product on coating/metal interface. These models can be used to obtain solution resistance, R_s, coating resistance, R_{pf}, coating capacitance, C_c, double layer capacitance C_{dl}, charge transfer resistance, R_{ct}, and Warburg resistance, Z_w.

Fig. 5(a)-(d) depicts the Nyquist plots for all the coating samples (EP, ESi, EZn and EZr) after one day exposure to 3.5 wt% NaCl. From the plot, it is well established that the pristine epoxy coating (Fig. 5(a)) initially dominates coating capacitance for higher values of frequencies and coating resistance for low values of frequencies during impedance studies. The resistive component is greater than $1\times10^9\ \Omega\ cm^2$. The absorption of ions from the surroundings greatly affects the resistance of the coating because it facilitates the transport of charge inside the coating. Therefore, based on the coating resistance, the anticorrosive performance of the film can be predicted [45].

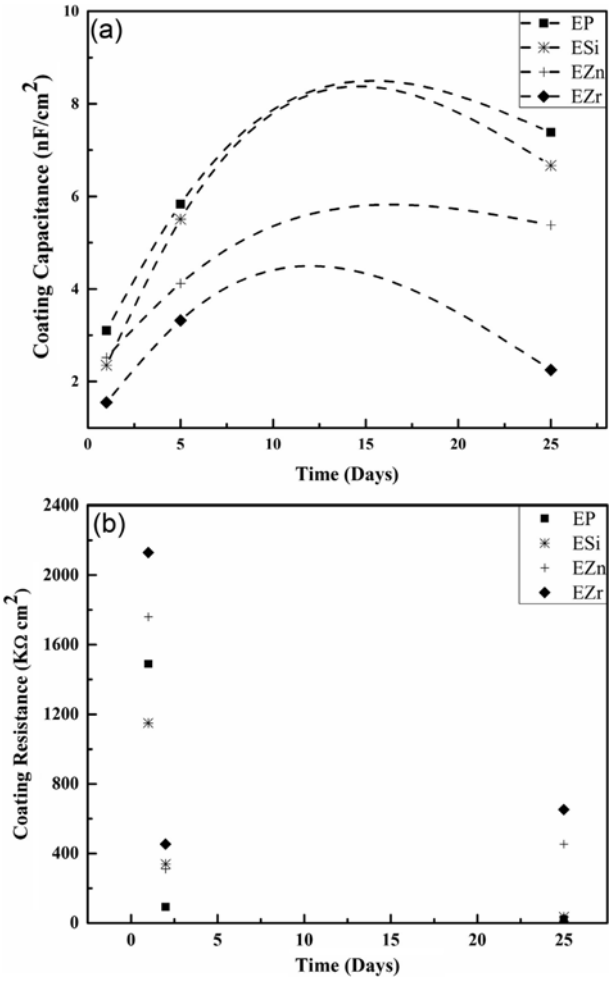

Fig. 9. (a) Time dependence of coating resistance and (b) time dependence of coating capacitance, for epoxy coating containing various nanoparticles coating on mild steel during 25 days immersion in 3.5% NaCl solution.

Fig. 9(a)-(b) shows the coating resistance and coating capacitance for all the samples after various intervals of exposure to corrosive electrolyte. The figure illustrates that the coating resistance for all the samples was reduced after exposure, which can be attributed to the infiltration and diffusion of ions and water inside the film resulting in enhanced coating conductivities [46]. The appearance of a second semicircle for the neat coating film (Fig. 5(a)) after five days of exposure reveals that the electrolyte diffused into the film through pores and reached the film/metal interface. The electrochemical reaction can be expected at the film/coating interface, where the conductive pathways through coating film enter the metal surface and the metal is exposed to the electrolyte. A significant decrease in the coating resistance is observed at this stage and, as a result, the increase in coating capacitance is revealed as given in Fig. 9(a)-(b). As a result of electrochemical reaction at the metal/coating interface, an inductive loop is obtained at low frequencies, which can be ascribed to a monolayer appearance at the surface as a result of corrosion products. This layer protects the surface from further corrosion and the phenomenon is known as passivation [45]. The huge decrease in the resistive component as 140 MΩ cm^2 and low impedance value after 25 days of immersion indicates the neat epoxy coating is not suitable for corrosive environment due to its poor corrosion resistance.

The results for EIS measurement of ESi sample follow the same pattern with a capacitance dominating behavior at high frequencies and coating resistance in the low frequency ranges with a resistive component of 1×10^9 Ω cm^2 after one day of immersion, which is almost the same as for the neat epoxy. After five days of immersion (Fig. 6(b)), a Warburg component appears at the end of the low frequency part of the graph. The appearance of the Warburg component reveals that the ions are diffused on the surface of the substrate and form corrosive species [47]. Here the polarization is due to a combination of kinetic and diffusion processes. After 25 days of immersion, the decrease in coating resistance is due to the penetration of electrolyte in the coating film. As a result, coating resistance is increased as shown in Fig. 9(a)-(b).

The initial behavior of EIS spectra obtained for EZn is the same as ESi with capacitive behavior for high frequency scan and resistive property for low frequency values. However, high resistive component (2.3 GΩ cm^2) is observed initially after one day of immersion. Eventually, after the exposure to corrosive environment is prolonged, the coating resistance decreases. The coating resistance and impedance values observed for EZn are higher than EP and ESi, which demonstrates the barrier properties ZnO NPs in the coating. The appearance of Warburg component after five days of exposure to the electrolyte is due to the diffusion of ions and water, thus forming corrosive species on the surface of the metal. The resistive component is reduced to 31 MΩ cm^2. However, after 25 days of exposure the Warburg component is stable and the resistive behavior remains dominant, indicating barrier properties of EZn.

EZr resulted in high resistive component and low coating capacitance of 1.2 nF cm^{-2}. The coating resistance on exposure to 3.5% NaCl solution decreased after five days of immersion. Nevertheless, it becomes somewhat stable after 25 days of immersion, which reveals that the incorporation of ZrO_2 NPs significantly reduced the corrosion rate compared with the neat epoxy sample and other nanocomposite coatings. The ohmic resistance and barrier properties may be responsible for the delay in penetration of oxygen, water and ions inside the coating film. Consequently, a reduction in the corrosion rate takes place and the single capacitive loop on the Nyquist plot is used to describe the phenomenon. For a prolonged immersion of EZr sample for 25 days in 3.5% NaCl solution, the ohmic resistance is much higher and stable for a longer period of time as shown in Fig. 7(d). Therefore, it can be said that EZr, as compared to other coating samples, demonstrates better anticorrosion properties. Nevertheless, the slight decrease in the coating resistance may be due to the improper fabrication of coating film, as the viscosity and presence of volatile solvents during application of film and curing process may cause some porosity in the film [48].

4. AFM Microstructure Analysis

The surface of neat epoxy and nanoparticle modified epoxy coating was studied by AFM using noncontact mode. This is well supported by the AFM topography height images of neat epoxy, which indicates coating surface was smooth with nanoscale roughness.

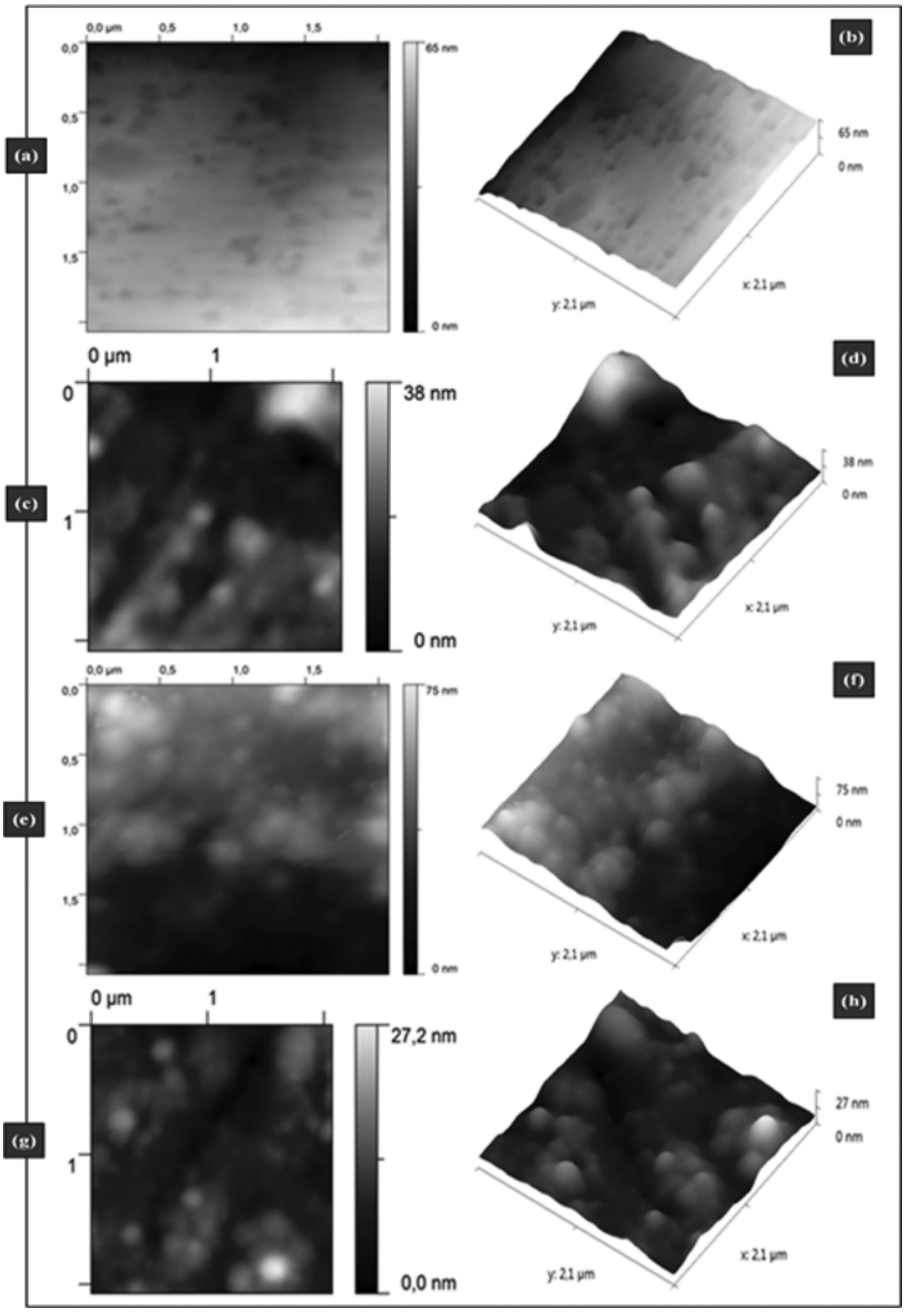

Fig. 10. Two- and three-dimensional surface morphology of unexposed coating surface, pristine epoxy (a), (b), EZn (c), (d), ESi (e), (f), EZr (g), (h).

The root mean square (RMS) surface roughness of 20 nm (EP), 26 nm (ESi), 25 nm (EZn), 23 nm (EZr) were obtained within the scanning area 2×2 µm for all the coating samples. As observed in Fig. 10, the addition of NPs increases the surface roughness of the coating. However, the difference in surface roughness of these coatings reveals that the density, shape of the NPs and their interaction with epoxy matrix may be responsible for the surface properties of the coating. ESi accounts for the highest surface roughness, which may be due to the lowest density (2.4 g/cm^3) of SiO_2 NPs as compared to others. The NPs may float on the surface while leaving traces behind after complete evaporation of the solvent. In contrast, EZn and EZr resulted in comparatively smooth surfaces due to their higher densities of 5.606 g/cm^3 and 5.89 g/cm^3, respectively. Increase in surface roughness may be attributed to the presence of NPs on surface of the coating. Topographic AFM images (phase images) of the coatings are shown in Fig. 10. These AFM images can be studied to analyze the homogeneous/heterogeneous dispersion of the NPs in epoxy matrix [49,50]. As can be observed, pristine sample has only one phase in contrast to the coating samples filled with 2 wt% of NPs consist of two phases.

The phases can be differentiated as light dots and dark parts on the surface. The light dots may be attributed to the nanoparticles.

Uniform distribution of these dots may reflect uniform dispersion of the NPs in the samples. These observations agree with SEM and EIS studies. NPs aggregation can cause decrease in surface particles' concentration and therefore surface roughness [51,52].

CONCLUSIONS

Possible chemical interactions between epoxy matrix and nano-particles in nano-composites coating enhance barrier properties and ionic resistances of developed coating as compared to the neat coating. Effect of nano-particles of ZnO, SiO_2 and ZrO_2 addition on the corrosion and morphology of the composite coating was investigated. It was found that addition of small concentration of all these NPs can improve the anti-corrosion properties of epoxy coatings as compared to the neat coating system. However, the addition of ZrO_2 resulted in significant improvement in the anticorrosion performance of epoxy coating as compared to other nano-composites coatings.

ACKNOWLEDGEMENT

The authors gratefully acknowledge the financial support from Center of Excellence in Engineering Materials (CEREM), Advanced Manufacturing Institute (AMI), King Saud University, P. O. Box 800, Riyadh-11421, Saudi Arabia.

REFERENCES

1. E. Bardel, *Corrosion and Protection*, Springer, London (2003).
2. E. S. Ferreira, C. Giacomelli, F. C. Giacomelli and A. Spinelli, *Mater. Chem. Phys.*, **83**, 129 (2004).
3. M. M. Popović, B. N. Grgur and V. B. Mišković-Stanković, *Prog. Org. Coat.*, **52**, 359 (2005).
4. B. D. Pennington, J. C. Grunlan and M. W. Urban, *J. Coating. Technol.*, **71**, 135 (1999).
5. M. Ates, *J. Adhes. Sci. Technol.*, **30**, 1510 (2016).
6. H. Leidheiser Jr., *Corrosion.*, **38**, 374 (1982).
7. G. A. Walter, *Corros. Sci.*, **26**, 27 (1986).
8. E. P. M. Van Westing, G. M. Ferrari and J. H. W. De Wit, *Corros. Sci.*, **34**, 1511 (1993).
9. S. E. Hörnström, J. Karlsson, W. J. Van Ooij, N. Tang and H. Klang, *J. Adhes. Sci. Technol.*, **10**, 883 (1996).
10. W. G. Ji, J. M. Hu, L. Liu, J. Q. Zhang and C. N. Cao, *J. Adhes. Sci. Technol.*, **22**, 77 (2008).
11. N. C. Rosero-Navarro, S. A. Pellice, A. Durán and M. Aparicio, *Corros. Sci.*, **20**, 1283 (2008).
12. T. C. Huang, Y. A. Su, T. C. Yeh, H. Y. Huang, C. P. Wu, K. Y. Huang, Y. C. Chou, J. M. Yeh and Y. Wei, *Electrochim. Acta*, **56**, 6142 (2011).
13. L. Ma, F. Chen, Z. Li, M. Gan, J. Yan, S. Wei, Y. Bai and J. Zeng, *Compos. Part B-Eng.*, **58**, 54 (2014).
14. H. Shi, F. Liu, L. Yang and E. Han, *Prog. Org. Coat.*, **62**, 359 (2008).
15. P. P. Mahulikar, R. S. Jadhav and D. G. Hundiwale, *Iran. Polym. J.*, **20**, 367 (2011).
16. A. C. Balaskas, I. A. Kartsonakis, L. A. Tziveleka and G. Kordas, *Prog. Org. Coat.*, **74**, 418 (2012).
17. N. Kouloumbi, G. M. Tsangaris, C. Vourvahi and F. Molnar, *J. Coat. Technol.*, **69**, 53 (1997).
18. L. Veleva, J. Chin and B. Del Amo, *Prog. Org. Coat.*, **36**, 211 (1999).
19. M. Rashvand, Z. Ranjbar and S. Rastegar, *J. Electrochem. Soc.*, **159**, C129 (2012).
20. S. K. Dhoke, A. Khanna and T. J. M. Sinha, *Prog. Org. Coat.*, **64**, 371 (2009).
21. A. Ehsani, M. Ghasem Mahjani, M. Nasseri and M. Jafarian, *Anti-Corros. Method. M.*, **61**, 146 (2014).
22. S. K. Dhoke, T. J. M. Sinha and A. Khanna, *J. Coat. Technol. Res.*, **6**, 353 (2009).
23. G. Gusmano, G. Montesperelli, M. Rapone, G. Padeletti, A. Cusmà, S. Kaciulis and A. Mezzi, *Surf. Coat. Technol.*, **201**, 5822 (2007).
24. M. Alexandre and P. Dubois, *Mat. Sci. Eng. R.*, **28**, 1 (2000).
25. D. J. Chaiko and A. A. Leyva, *Chem. Mater.*, **17**, 19 (2005).
26. M. Sabzi, S. Mirabedini, J. Zohuriaan-Mehr and M. Atai, *Prog. Org. Coat.*, **65**, 222 (2009).
27. M. Gerosa, A. Sacco, A. Scalia, F. Bella, A. Chiodoni, M. Quaglio, E. Tresso and S. Bianco, *IEEE J. Photovolt.*, **6**, 498 (2016).
28. F. Bella, A. Sacco, G. Massaglia, A. Chiodoni, C. F. Pirri and M. Quaglio, *Nanoscale.*, **7**, 12010 (2015).
29. F. Bella, G. Leftheriotis, G. Griffini, G. Syrrokostas, S. Turri, M. Grätzel and C. Gerbaldi, *Adv. Funct. Mater.*, **26**, 1127 (2016).
30. P. Im, Y. J. Choi, W. J. Yoon, D. G. Kang, M. Park, D. Y. Kim, C. R. Lee, S. Yang, J. H. Lee, K. Jeong, *Sci. Rep.*, **6**, 36472 (2016).
31. D. Pintossi, G. Iannaccone, A. Colombo, F. Bella, M. Välimäki, K. L. Väisänen, J. Hast, M. Levi, C. Gerbaldi, C. Dragonetti, S. Turri and G. Griffini, *Adv. Electron. Mater.*, **2**, 1600288 (2016).
32. M. Nakagawa, A. Nakaya, Y. Hoshikawa, S. Ito, N. Hiroshiba and T. Kyotani, *ACS Appl. Mater. Interfaces.*, **8**, 30628 (2016).
33. B. Ramezanzadeh, M. M. Attar and M. Farzam, *Prog. Org. Coat.*, **72**, 410 (2011).
34. B. Ramezanzadeh and M. M. Attar, *Prog. Org. Coat.*, **71**, 242 (2011).
35. Z. M. Huang, *Mater. Sci. Technol.*, **16**, 81 (2000).
36. B. Ramezanzadeh, M. M. Attar and M. Farzam, *J. Therm. Anal. Calorim.*, **103**, 731 (2011).
37. B. Ramezanzadeh and M. M. Attar, *Mater. Chem. Phys.*, **130**, 1208 (2011).
38. B. Ramezanzadeh, M. M. Attar and M. Farzam, *Prog. Org. Coat.*, **72**, 410 (2011).
39. R. Khan, M. R. Azhar, A. Anis, M. A. Alam, M. Boumaza and S. M. Al-Zahrani, *J. Coat. Technol. Res.*, **13**, 159 (2016).
40. J. Wu, J. Xie, L. Ling, G. Ma and B. Wang, *J. Coat. Technol. Res.*, **10**, 849 (2013).
41. J. Choi, S. G. Kim and R. M. Laine, *Macromolecules.*, **37**, 99 (2004).
42. J. W. Gilman, C. L. Jackson, A. B. Morgan, R. Harris, E. Manias, E. P. Giannelis, M. Wuthenow, D. Hilton and S. H. Phillips, *Chem. Mater.*, **12**, 1866 (2000).
43. Z. Peng, L. X. Kong and S. D. Li, *J. Appl. Polym. Sci.*, **96**, 1436 (2005).
44. S. C. Hsu, W. T. Whang, C. H. Hung, P. C. Chiang and Y. N. Hsiao, *Macromol. Chem. Phys.*, **206**, 291 (2005).
45. S. M. Mirabedini, G. E. Thompson, S. Moradian and J. D. Scantlebury, *Prog. Org. Coat.*, **46**, 112 (2003).
46. M. Niknahad, S. Moradian and S. M. Mirabedini, *Corros. Sci.*, **52**, 1948 (2010).
47. G. W. Walter, *Corros. Sci.*, **26**, 681 (1986).
48. S. M. Mirabedini, M. Behzadnasab and K. Kabiri, *Compos. Part A-*

Appl. S., **43**, 2095 (2012).
49. M. Salmerón Sánchez, J. Molina Mateo, F. J. Romero Colomer and J. L. Gómez Ribelles, *Eur. Polym. J.*, **42**, 1378 (2006).
50. D. K. Chattopadhyay, A. J. Muehlberg and D. C. Webster, *Prog. Org. Coat.*, **63**, 405 (2008).
51. S. W. Kim, *Korean J. Chem. Eng.*, **25**, 1195 (2008).
52. S. W. Kim, *Korean J. Chem. Eng.*, **28**, 298 (2011).